Theoretical Study and Rate Constant Computation on the Reaction HFCO + OH → CFO + H_2O

Chaoyang Wang and Qian Shu Li*

Center for Computational Quantum Chemistry and School of Chemistry & Environment, South China Normal University, Guangzhou 510006, People's Republic of China, and Institute for Chemical Physics, Beijing Institute of Technology, Beijing, 100081, People's Republic of China

Received: April 3, 2007; In Final Form: September 1, 2007

The potential energy surface, including the geometries and frequencies of the stationary points, of the reaction HFCO + OH is calculated using the MP2 method with 6-31+G(d,p) basis set, which shows that the direct hydrogen abstraction route is the most dominating channel with respect to addition and substitution channels. For the hydrogen abstraction reaction, the single-point energies are refined at the QCISD(T) method with 6-311++G(2df,2pd) basis set. The calculated standard reaction enthalpy and barrier height are −17.1 and 4.9 kcal mol^{-1}, respectively, at the QCISD(T)/6-311++G(2df,2pd)//MP2/6-31+G(d,p) level of theory. The reaction rate constants within 250−2500 K are calculated by the improved canonical variational transition state theory (ICVT) with small-curvature tunneling (SCT) correction at the QCISD(T)/6-311++G(2df,2pd)//MP2/6-31+G(d,p) level of theory. The fitted three-parameter formula is $k = 2.875 \times 10^{-13}(T/1000)^{1.85}$ exp(−325.0/*T*) cm^3 $molecule^{-1}$ s^{-1}. The results indicate that the calculated ICVT/SCT rate constant is in agreement with the experimental data, and the tunneling effect in the lower temperature range plays an important role in computing the reaction rate constants.

1. Introduction

Due to the adverse impact of chlorofluorocarbons (CFCs) on stratospheric ozone and the greenhouse effect, an international agreement has been undertaken to remove CFCs from large-scale industrial production and replace them with environmentally acceptable alternatives.[1−3] Hydrofluorocarbons (HFCs) are one class of potential CFC substituents because they have no potential for ozone depletion.[4] In addition, these compounds, having carbon−hydrogen bonds, can be oxidized in the atmosphere by highly reactive radical species, such as OH radicals.[5] Therefore, the study of the rate constants and dynamics of these small molecules is of interest to both experimentalists and theoreticians. Considerable attention has been paid to the reactions of HFCs with OH radical.[6,7]

HFCO is one of the main oxidation products of several HFCs, such as CH_2FCH_2F, CH_3F, and CF_3CFH_2.[4] An expected tropospheric removal route for HFCO is by reaction with OH radicals via a hydrogen abstraction mechanism.[8] The dynamics for the reaction HFCO + OH → CFO + H_2O has previously been studied experimentally and theoretically. Wallington et al.[9] gave the rate constant $k = 4 \times 10^{-15}$ cm^3 $molecule^{-1}$ s^{-1} at 298 K by means of a photolysis technique, Atkinson et al.[6] estimated the upper limit of the rate constant to be 1.00×10^{-14} cm^3 $molecule^{-1}$ s^{-1} at 298 K, and Francisco[8] reported the rate constant to be $k = 7.0 \times 10^{-16}$ cm^3 mol^{-1} s^{-1} with the PMP4SDTQ/6-311++G(d,p)//UMP2/6-311G(d,p) method at 299.3 K. The great differences in the above rate constants for the title reaction prompt us to further study it. In the present work, we attempted to perform a dual-level QCISD(T)/6-311++G(2df,2pd)//MP2/6-31+G(d,p) calculation to obtain more reasonable rate constants and to predict the activation energies of the title reaction.

2. Calculational Methods

2.1. Electronic Structure Calculations. The geometries and frequencies of all stationary points (reactants, products, intermediates, and the transition states) are optimized at the MP2/6-31+G(d,p) level of theory. MP2 denotes the second-order Møller−Plesset[10−12] perturbation theory. The minimum energy path (MEP)[13] is calculated using the intrinsic reaction coordinate (IRC) theory[14] in mass-weighted Cartesian coordinates with a gradient step size of 0.03 $amu^{1/2}$ bohr at the MP2/6-31+G(d,p) level of theory. The force constants and Hessians for the selected points along the MEP were obtained at the MP2/6-31+G(d,p) level of theory. For the title reaction, the QCISD(T)/6-311++G(2df,2pd) was employed to refine the energies of the stationary points and selected points along the MEP. Here QCISD(T) is referred to as the quadratic configuration interaction (CI) calculation including single and double substitutions with a triple contribution to the energy added.[15] All the above calculations are performed using the Gaussian 03 system of programs.[16]

2.2. Rate Constant Calculations. The rate constants are calculated using the conventional transition state theory (TST) and improved canonical variational transition state theory (ICVT).[17] The ICVT is used in order to treat the threshold region as accurately as in the microcanonical variational theory.

The expression of the improved generalized-transition-state-theory rate constant is written as

$$k^{\mathrm{IGT}}(T,s) = [h\Phi^{\mathrm{R}}(T)]\int_{V_a^{\mathrm{G}}}^{\infty} \mathrm{d}E\ \mathrm{e}^{-\beta E} N^{\mathrm{GT}}(E,s)$$

h is Planck's constant; $\Phi^{\mathrm{R}}(T)$ is the partition function per unit volume; $\beta = 1/(k_{\mathrm{B}}T)$, where k_{B} is Boltzmann's constant; V_a^{G} is the maximum of the vibrationally adiabatic ground-state potential energy curve; and $N^{\mathrm{GT}}(E,s)$ is the quantized cumulative reaction probability at energy E and reaction coordinate s. The

10.1021/jp0725937 CCC: $40.75 © 2008 American Chemical Society
Published on Web 12/29/2007

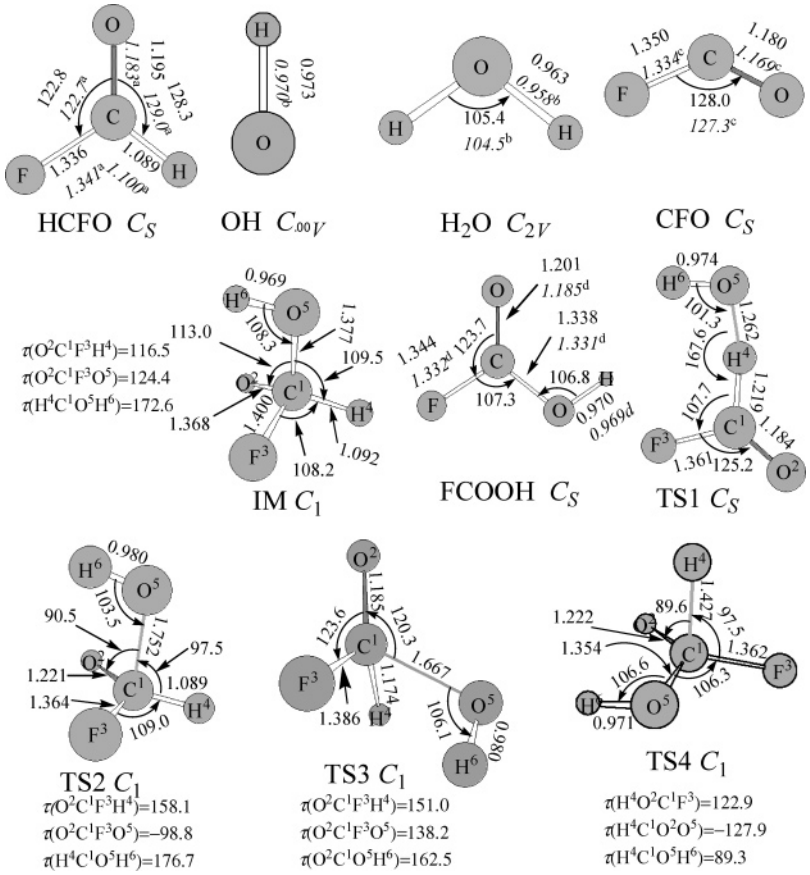

Figure 1. Geometric parameters (distances in angstroms and angles in degrees) of the equilibrium and transition state structures for the HCFO + OH reaction at the MP2/6-311+G(d,p) level. Note: [a]ref 23; [b]ref 24; [c]ref 25; [d]ref 26.

ICVT dividing surface is located to minimize the improved generalized-transition-state-theory rate constant, i.e.

$$\frac{\partial k^{\mathrm{IGT}}(T,s)}{\partial s}|_{s=s_{*}{}^{\mathrm{ICVT}}(T)} = 0$$

The threshold for reaction in the improved canonical variational theory is V_a [$n = 0$, $s = s_{*}{}^{\mathrm{ICVT}}(T)$].

Furthermore, the ICVT rate constants are corrected with the small-curvature tunneling (SCT) transmission coefficient.[18−20] The SCT transmission coefficients, which include the reaction-path curvature effect on the transmission probability, are based on the centrifugal-dominant small-curvature semiclassical adiabatic ground-state approximation. In particular, the transmission probability at energy E is given by

$$P(E) = \frac{1}{1 + \exp[-2\theta(E)]}$$

where $\theta(E)$ is the imaginary action integral evaluated along the reaction coordinate

$$\theta(E) = \frac{2\pi}{h}\int_{S_1}^{S_r}\sqrt{2\mu_{\mathrm{eff}}(s)|E - V_a{}^{G}(s)|}\,\mathrm{d}s$$

in which the integration limits S_1 and S_r are the reaction coordinate classical turning points. The effect of the reaction-path curvature on the tunneling probability is included in the effective reduced mass, μ_{eff}.

The rate constants of the title reaction are computed using three levels of theory, namely, the conventional transition state theory (TST), the improved canonical varitional transition state theory (ICVT), and the improved canonical varitioanl transition state theory with small-curvature tunneling correction (ICVT/SCT), respectively. In the present work, all the vibrational modes are treated as quantum-mechanically separable harmonic oscillators except for the lowest vibrational two. The hindered rotor approximation of Truhlar and Chuang[21] is used to calculate the partition function of the lowest mode. The evaluations of the rate constants are performed employing the Polyrate 9.4 program.[22]

3. Results and Discussion

3.1. Stationary Points. Theoretical investigations of the HCFO + OH reaction suggest that there exist three kinds of reaction channels:

$$\mathrm{HCFO + OH \rightarrow CFO + H_2O} \quad \text{(R1)}$$

$$\mathrm{HCFO + OH \rightarrow HCFOOH\ (IM) \rightarrow FCOOH + H} \quad \text{(R2)}$$

$$\mathrm{HCFO + OH \rightarrow FCOOH + H} \quad \text{(R3)}$$

namely "direct hydrogen abstraction (R1)", "hydroxyl addition (R2)", and "hydroxyl substitution (R3)" channels. Four transition states (TSs), TS1 corresponding to the products CFO + H_2O (R1), TS2 and TS4 to corresponding to FCOOH + H (R2), TS3 corresponding to FCOOH + H (R3), and an intermediate HCFOOH (R2) are located.

Figure 1 shows the optimized geometric parameters of the stationary points, including the reactants, products, and transition states as well as the intermediates, at the MP2/6-31+G(d,p) level of theory along with the available experimental data.[23−26] It can be seen that the theoretical geometric parameters of OH, HCFO, H_2O, CFO, and FCOOH are in good agreement with the

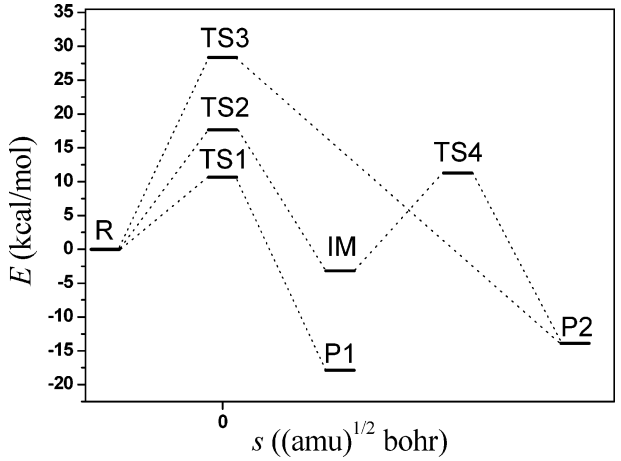

Figure 2. Schematic pathways for the HCFO + OH reaction. Relative energies (in kcal/mol) are calculated at the MP2/6-31+G(d,p) + ZPE level.

corresponding experimental values. The largest deviation of the bond length is 0.016 Å of C^1-F^3 in HFCO, and that of the bond angles is 0.9° of $H^4-O^5-H^6$ in H_2O. For the transition state (TS1), the bond C^1-H^4, which will be broken, is elongated by 0.130 Å with respect to the equilibrium bond length in HFCO; the distance of the H^4-O^5 bond, which will be formed, is 0.299 Å longer than that in the free H_2O. This means that the transition state structure is more reactant-like, and the reaction will proceed via an early transition state. This is the expected behavior of Hammond's postulate for exothermic reactions.

A schematic potential energy surface of the CHFO + OH reaction is plotted in Figure 2 at the MP2/6-31+G(d,p) level. As shown in Figure 2, the addition of OH to HCFO produces HCFOOH radical, which lies about 12.0 kcal mol^{-1} below the reactants in energy. HCFOOH can decompose to yield H atom and FCOOH molecule via TS4, and it is found that TS4 is over 11.0 kcal mol^{-1} higher than reactants. However, the elimination TS is not obtained from the intermediated HCFOOH to the products CFO and H_2O in this work. The barrier heights of the addition and substitution routes are higher than that of the hydrogen abstraction pathway by above 7.0 and 18.0 kcal mol^{-1}, respectively. Therefore, for the reaction HCFO + OH, the direct hydrogen abstraction is the most favorable channel, while the addition and substitution routes are much less competitive than the direct hydrogen abstraction route. The R1 energetics information including the reaction energy (ΔE), the reaction enthalpy ($\Delta H_{298\,K}°$), the forward classical potential barrier ($V^{\ddagger}$), and the vibrationallly adiabatic ground-state potential barrier ($V_a^{G\ddagger}$) are listed in Table 1. It can be seen that the predicted reaction enthalpy (−17.1 kcal mol^{-1}) at the QCISD(T)/6-311++G(2df,2pd)/MP2/6-31+G(d,p) level of theory is about 2.2 kcal mol^{-1} larger than the experimental value[27] (−19.3 kcal mol^{-1}), but it is much closer to the Francisco result[8] (−17.4 kcal mol^{-1}). The obtained forward classical potential barrier height $V^{\ddagger}$ (4.9 kcal mol^{-1}) and the vibrationally adiabatic ground-state potential barrier $V_a^{G\ddagger}$ (3.2 kcal mol^{-1}) at the QCISD(T)/6-311++G(2df,2pd)//MP2/6-31+G(d,p) level of theory are much lower than the predicted corresponding values (8.4 kcal mol^{-1} and 6.0 kcal mol^{-1}) by Francisco at the PMP4SDTQ/6-311++G(d,p)//UMP2/6-311G(d,p) level of theory. In order to compare our theoretical values with the Francisco results, the QCISD(T)/6-311++G(2df,2pd)//QCISD/6-31+G(d,p) and CCSD(T)/6-311++G(2df,2pd)//CCSD/6-31+G(d,p) computations were performed. The obtained ΔE are −17.1 and −16.8 kcal mol^{-1}; $\Delta H_{298}°$ are −16.8 and −16.5 kcal mol^{-1}; $V^{\ddagger}$ are 4.8 and 5.2 kcal mol^{-1}; and $V_a^{G\ddagger}$ are 2.9 and 3.2 kcal mol^{-1}, respectively, at above two levels. These results show that our theoretical values should be available for the reaction of HFCO with OH.

The harmonic vibrational frequencies and zero-point energies of the reactants, transition states, intermediates, and products of the HCFO + OH reaction are listed in Table 2 at the MP2/

TABLE 1: Reaction Energetic Parameters (kcal mol^{-1}) of the Reaction HCFO + OH → CFO + H_2O at Different Levels of Theory

methods	ΔE	$V^{\ddagger}$	$V_a^{G\ddagger}$	$\Delta H_{298}°$
QCISD(T)/6-311++G(2df,2dp)//MP2/6-31+G(d,p)	−17.3	4.9	3.2	−17.1
QCISD(T)/6-311++G(2df,2dp)//QCISD/6-31+G(d,p)	−17.1	4.8	2.9	−16.8
CCSD(T)/6-311++G(2df,2dp)//CC/6-31+G(d,p)	−16.8	5.2	3.2	−16.5
exptl[a]				−19.3

[a] Reference 27.

TABLE 2: Harmonic Vibrational Frequencies (cm^{-1}) and Zero-Point Energies (kcal mol^{-1}) of Reactants, Intermediate, Transition States, and Products of the Reaction of HCFO with OH at the MP2/6-31+G(d,p) Level of Theory

species		frequencies (cm^{-1})	ZPE
HFCO	theor	3224, 1852, 1396, 1053, 1031, 643	13.2
	exptl[a]	2981, 1837, 1343, 1065, 1013, 663	
OH	theor	3825	5.5
	exptl[b]	3570	
CFO	theor	1995, 1038, 612	5.2
	exptl[c]	1862, 1026, 628	
H_2O	theor	4013, 3886, 1623	13.6
	exptl[b]	3765, 3651, 1595	
FCOOH	theor	3835, 1901, 1388, 1203, 949, 769, 602, 579, 552	16.8
	exptl[d]	3618, 1866	
HCFOOH	theor	3845, 3173, 1406, 1328, 1291, 1137, 1022, 956, 592, 518, 272, 194	22.5
TS1	theor	3806, 2001, 1516, 1051, 978, 845, 686, 473, 227, 134, 124, 2628i	16.9
TS2	theor	3739, 3225, 1682, 1397, 1159, 1073, 928, 666, 529, 370, 304, 923i	21.6
TS3	theor	3808, 3373, 2273, 1334, 1119, 1005, 922, 673, 530, 504, 358, 658i	22.7
TS4	theor	3850, 1839, 1304, 1178, 971, 847, 776, 746, 534, 521, 443, 1789i	18.6

[a] Reference 28. [b] Reference 29. [c] Reference 30. [d] Reference 26.

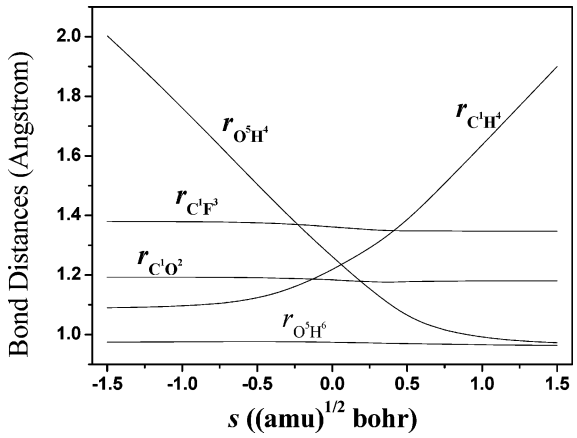

Figure 3. Changes of the main bond lengths (in angstroms) as functions of s (amu$^{1/2}$ bohr) at the MP2/6-31+G(d,p) level.

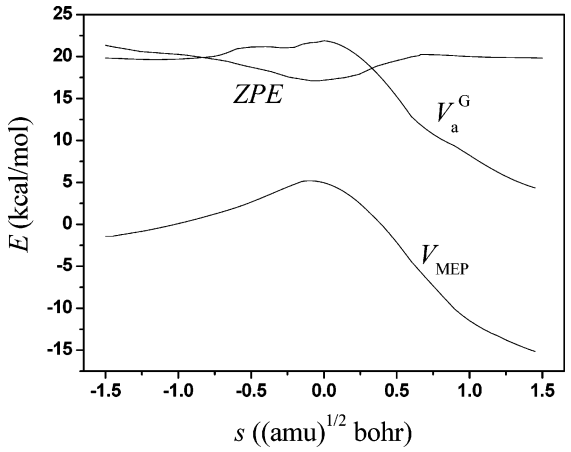

Figure 4. Classical potential energy V_{MEP}, zero-point energy (ZPE), and ground-state vibrationally adiabatic potential energy V_a^G as functions of s (amu$^{1/2}$ bohr) at QCISD(T)/6-311+G(2df,2pd)//MP2/6-31+G(d,p) level.

6-31+G(d,p) levels of theory along with the available experimental data.[25,28−30] It could be seen that the calculated harmonic vibrational frequencies of the reactants and the products were consistently larger than the corresponding experimental data. The most discrepancies between the theoretical results and experimental data are generally within 7.5%. This shows that the calculated frequencies are in agreement with the experimental data, and our theoretical frequencies are smaller than Francisco's reported data. It is well-known that the frequencies calculated by the MP2 method are larger than the experimental frequencies, and in principle, these theoretical frequencies should be rescaled, i.e., multiplied by a factor of about 0.88 to approach the experimental frequencies. Generally, the discrepancies of the rescaled theoretical results and experimental data could be within 5%. As mentioned above, the discrepancies of our results and the experimental data are close to this value. Also, the transition states obtained here are reactant-like transition states, which means that the structures of the transition states are closer to those of the reactants. It is guessed that, due to the calculated frequencies of both the reactants and transition states not being rescaled, the corresponding discrepancies might be partly counteracted; therefore, the frequencies are not rescaled in the present paper. In addition, it can be also seen that the transition state possesses only one imaginary frequency with the absolute value 2628 cm^{-1}, and the barrier is narrow; therefore, the tunneling correction in the calculation of the rate constants is significant.

3.2. Reaction-Path Properties. As analyzed above, the dominant pathway of the HCFO + OH reaction is the hydrogen abstraction by hydroxyl, i.e., HCFO + OH → CFO + H_2O (R1). In this section, only the reaction-path properties of reaction R1 are discussed.

Figure 3 shows the change of the bond distances (angstroms) along the minimum energy path as a function of reaction coordinate s (amu$^{1/2}$ bohr) at the MP2/6-31+G(d,p) level of theory. It is shown that the lengths of the breaking bond C^1−H^4 and the forming bond H^4−O^5 change strongly near the transition state (s = 0), while the other bond lengths remain almost unchanged in the course of the reaction. The change of the C^1−H^4 bond length remains invariant until the intrinsic reaction coordinate reaches about −0.50 amu$^{1/2}$ bohr, where it starts increasing sharply with increasing s. Meanwhile, the H^4−O^5 distance decreases rapidly until the intrinsic reaction coordinate reaches 0.75 amu$^{1/2}$ bohr. During this process, the C^1−H^4 bond breaks and the H^4−O^5 bond forms. The geometry changes mainly take place in the region about s = −0. 50 to + 0.75 amu$^{1/2}$ bohr.

TABLE 3: Bottleneck Properties Determined by the Transition State Theory (TST) and Improved Canonical Variational TST (ICVT) Methods for the HFCO + OH → CFO + H_2O Reaction

T (K)	s (bohr)	V_{MEP}	V_a^G
SP[a]	0.000	5.0	21.7
250.0	0.016	4.9	21.7
295.0	0.021	4.8	21.7
298.0	0.022	4.8	21.7
300.0	0.022	4.8	21.7
400.0	0.036	4.8	21.6
500.0	0.052	4.7	21.6
600.0	0.057	4.6	21.5
700.0	0.066	4.6	21.5
800.0	0.073	4.5	21.4
1000.0	0.085	4.4	21.4
1250.0	0.097	4.3	21.3
1500.0	0.105	4.2	21.2
1750.0	0.112	4.2	21.2
2000.0	0.118	4.1	21.1
2500.0	0.126	4.0	21.0

[a] The bottleneck properties of this row are based on conventional TST, and those of other rows are based on CVT.

The curves of the classical potential energy (V_{MEP}), ground-state vibrational adiabatic potential energy (V_a^G), and the zero-point energy (ZPE) along the MEP as functions of the intrinsic reaction coordinate (s) of the title reaction are presented in Figure 4 at the QCISD(T)/6-311++G(2df,2pd)//MP2/6-31+G-(d,p) level of theory. As shown in Figure 4, the $V_{MEP}(s)$ and the $V_a^G(s)$ energy curves of the reaction are very similar in shape. The position of the transition state does not greatly shift. To further investigate the variational effect in the computation of rate constants, the dynamic bottleneck properties of the title reaction based on the canonical variational transition state approach were calculated and are listed in Table 3. The bottleneck properties indicate the positions of the variational transition state deviated from the saddle point at s = 0.0 amu$^{1/2}$ bohr at various temperatures. It can be seen from Table 3 that the largest deviation in the temperature range 250−2500 K is at 2500 K, where s = 0.126 amu$^{1/2}$ bohr, and the corresponding V_{MEP} and V_a^G values are 4.0 and 21.0 kcal mol^{-1}, respectively. Since for the conventional transition state (s = 0), V_{MEP} and V_a^G take the values 5.0 and 21.7 kcal mol^{-1}, respectively, the largest deviations, $V_{MEP}(s{=}0.126) - V_{MEP}(s{=}0)$ = 1.0 kcal·mol^{-1} and $V_a^G(0.126) - V_a^G(s{=}0.000)$ = 0.7 kcal mol^{-1}, are very small. This implies that the configurations of the transition states and variational transition states are close, and the effect of

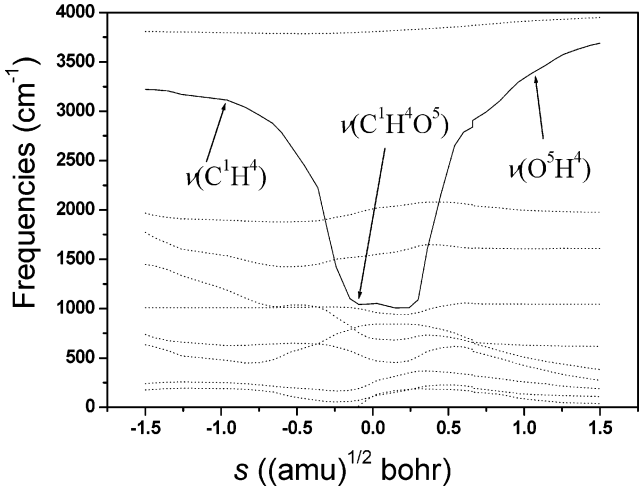

Figure 5. Changes of the generalized normal-mode vibrational frequencies as functions of s (amu$^{1/2}$ bohr) at the MP2/6-31+G(d,p) level.

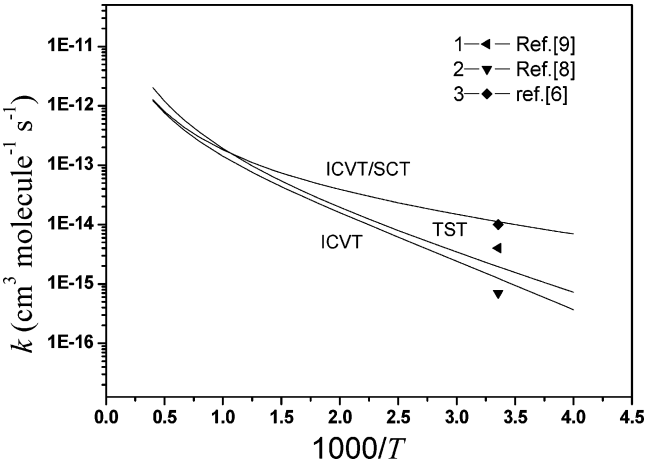

Figure 6. Reaction rate constants k (cm^3 molecule^{-1} s^{-1}) as a function of the reciprocal of the temperature (K^{-1}) over the temperature range 250−1600 K.

variational corrections on the calculation of the rate constant of the title reaction should not be obvious. In fact, variational TST is required to be used for (almost) barrierless reactions. The corresponding energy gradients around the TS location are small, and the structural parameters (and the derived rotational constants and low-frequency motions) are changing rapidly in this region. In the present reaction, the transition state structure is more reactant-like, the barrier height is not large, and the reaction will proceed via an early transition state. Here, the application of the improved canonical variational transition state theory could make us believe that the computational preexponential factors are more reliable.

Figure 5 describes the changes of the generalized normal-mode vibrational frequencies along the MEP at the MP2/6-31+G(d,p) level. In the negative limit of s, the frequencies are associated with the reactants, and in the positive limit of s, the frequencies are associated with the products. There are 11 vibrational frequencies in the vicinity of the transition state. For the vibrational mode $\nu(C^1-H^4-O^5)$ (solid line), it is connected to the stretching vibrational mode of the breaking C^1-H^4 bond when $s < 0$ amu$^{1/2}$ bohr. When $s > 0$ amu$^{1/2}$ bohr, the vibrational mode $\nu(C^1-H^4-O^5)$ is connected to the stretching vibrational mode of the H^4-O^5 bond. From Figure 5, it can be seen that the frequency of the vibrational mode $\nu(C^1-H^4-O^5)$ changes sharply in the range from $s = -0.50$ to $+0.75$ amu$^{1/2}$ bohr, which is similar to the range of the distance changes of the breaking and forming bonds in Figure 3. Therefore, the mode $\nu(C^1-H^4-O^5)$ can be referred to as the "reactive mode". Most of the other frequencies do not change significantly on going from the reactants to products.

3.3. Rate Constant Calculation. The TST, ICVT, and ICVT/SCT are employed to calculate the rate constants for the HFCO + OH → CFO + H_2O reaction in the temperature range 250−2500 K. The rate constants and the corresponding experimental values are listed in Table 4. Figure 6 plots both the theoretical and experimental[6,8,9] rate constants versus 1000/T (K^{-1}) for the title reaction. From Figure 6, it could be seen that the rate constants of ICVT/SCT are close to the experimental data in ref 6, but they are higher than the experimental data in ref 9. Francisco's reported rate constants are the lowest with respect to refs 6 and 9 as well as our theoretical values. This indicates that Francisco's predicted barrier height (8.4 kcal mol^{-1}) with the PMP4SDTP/6-311++G(d,p)//UMP2/6-311G(d,p) method is too high for the title reaction. The difference between the TST and ICVT rate constants is quite small, which indicates that the improved canonical variational effect is very small for the calculation of the rate constants. At 250 K, the ICVT/SCT rate constant is larger than that of ICVT by a factor of more than 18.0. As the temperature increases, the predicted ICVT rate constant becomes consistent with the ICVT/SCT rate constant. These indicate that the small-curvature tunneling effect

TABLE 4: Forward Reaction Rate Constants (cm^3 molecule^{-1} s^{-1}) of the HFCO + OH → CFO + H_2O Reaction in the Temperature Range 250−2500 K

T (K)	TST	ICVT	ICVT/SCT
250.00	7.25×10^{-16}	3.68×10^{-16}	6.97×10^{-15}
295.00	1.86×10^{-15}	1.16×10^{-15}	1.09×10^{-14}
298.00[a]	1.96×10^{-15}	1.24×10^{-15}	1.14×10^{-14}
305.00	2.21×10^{-15}	1.43×10^{-15}	1.19×10^{-14}
350.00	4.36×10^{-15}	3.15×10^{-15}	1.68×10^{-15}
400.00	7.95×10^{-15}	6.15×10^{-15}	2.33×10^{-14}
500.00	1.96×10^{-14}	1.59×10^{-14}	3.90×10^{-14}
600.00	3.80×10^{-14}	3.08×10^{-14}	5.84×10^{-14}
700.00	6.39×10^{-14}	5.08×10^{-14}	8.26×10^{-14}
800.00	9.79×10^{-14}	7.60×10^{-14}	1.10×10^{-13}
1000.00	1.92×10^{-13}	1.42×10^{-13}	1.81×10^{-13}
1250.00	3.59×10^{-13}	2.52×10^{-13}	2.95×10^{-13}
1500.00	5.83×10^{-13}	3.92×10^{-13}	4.39×10^{-13}
1750.00	8.63×10^{-13}	5.61×10^{-13}	6.10×10^{-13}
2000.00	1.20×10^{-12}	7.57×10^{-13}	8.07×10^{-13}
2500.00	2.02×10^{-12}	1.22×10^{-12}	1.27×10^{-12}

[a] Experimental values are 1.00×10^{-14} from ref 6 and 4.00×10^{-15} for ref 9, and the previously computed value is 7.0×10^{-16} for ref 8.

is significant at low temperature. Furthermore, the forward ICVT/SCT rate constants within 250−2500 K are fitted by the three-parameter expression in units of cm^3 $molecule^{-1}$ s^{-1} as follows:

$$k = 2.875 \times 10^{-13}(T/1000)^{1.85} \exp(-325.0/T)$$

In the present work, the discrepancies of the computational and realistic reaction rate constants seem to be mainly originated from the errors of the calculated potential energy surface. Although the curvature and tunneling effects of barrier have been partly corrected, the rescaling of frequencies and nonharmonic properties of the vibrations are not still taken into consideration.

4. Summary

The geometries and frequencies of all stationary points, containing the reactants, products, intermediates, and transition states, as well as the potential energy surface for the reaction HFCO + OH are calculated at the MP2/6-31+G(d,p) level of theory. It is shown that, in terms of the potential energy surface, the dominant reaction pathway is the direct hydrogen abstraction process which forms the products CFO and H_2O, while addition and substitution routes leading to the products FCOOH and H atom are less competitive. For the hydrogen abstraction, the theoretical standard reaction enthalpy (−17.1 kcal mol^{-1}), the classical barrier height (4.9 kcal mol^{-1}), and the vibrationally adiabatic ground-state potential barrier (3.2 kcal mol^{-1}) have been predicted at the QCISD(T)/6-311++G(2df,2pd)//MP2/6-31+G(d,p) level of theory. The changing curves of the bond distances and frequencies along the minimum energy path are obtained by means of the MP2/6-31+G(d,p) method. The curve of potential energy along the minimum energy path is obtained using the QCISD(T)/6-311++G(2df,2pd)//MP2/6-31+G(d,p) method. The reaction thermal rate constants for the reaction HFCO + OH → CFO + H_2O in the temperature range 250−2500 K are calculated by the TST, ICVT, and ICVT/SCT methods. The ICVT/SCT rate constant at 298 K is very close to the experimental data[6] and different from the previously theoretical[8] and experimental[9] data. The corresponding fitted three-parameter expression for the reaction rate constants within 250−2500 K is $k = 2.875 \times 10^{-13}(T/1000)^{1.85} \exp(-325.0/T)$ for the title reaction. In the low-temperature region, the curvature of the ICVT/SCT rate constants is larger than those obtained by using the TST and ICVT theories. These indicate that the small-curvature tunneling effect makes important contributions in the calculation of rate constants in the low-temperature region.

Acknowledgment. The authors thank Prof. Donald G. Truhlar for providing the Polyrate 9.4.1 program. This work is supported by the National Science Foundation of China and by the 111 project (B07012) in China.

References and Notes

(1) Farman, J. D.; Gardiner, B. G.; Shanklin, J. D. *Nature* **1985**, *315*, 207.
(2) Soloman, S. *Nature* **1990**, *347*, 6291, and references therein.
(3) *Scientific Assessment of Stratospheric Ozone*; World Meteorological Organization Global Ozone Research and Monitoring Project, Report No. 20; 1989; p 1.
(4) Wu, J. *Chem. Phys. Lett.* **2002**, *369*, 504.
(5) Fontanna, G. *J. Fluorine Chem.* **2001**, *109*, 113.
(6) Atkinson, R.; Baulch, D. L.; Cox, R. A.; Hampson, R. F., Jr.; Kerr, J. A.; Rossi, M. J.; Troe, J. *J. Phys. Chem. Ref. Data* **1997**, *26*, 521.
(7) Atkinson, R. *J. Phys. Chem. Ref. Data* **1994**, Monograph No. 2.
(8) Francisco, J. S. *J. Chem. Phys.* **1992**, *96*, 7597−7601.
(9) Wallington, T. J.; Hurley, M. D. *Environ. Scl. Technol.* **1993**, *27*, 1452.
(10) Head-Gordon, M.; Head-Gordon, T. *Chem. Phys. Lett.* **1994**, *220*, 122; *J. Chem. Phys.* **1995**, *103*, 962.
(11) Frisch, M. J.; Head-Gordon, M.; Pople, J. A. *Chem. Phys. Lett.* **1990**, *166*, 275.
(12) Head-Gordon, M.; Pople, J. A.; Frisch, M. J. *Chem. Phys. Lett.* **1988**, *153*, 503.
(13) Fukui, K. *J. Phys. Chem.* **1970**, *74*, 4164.
(14) Gonzalez, C.; Schlegel, H. B. *J. Chem. Phys.* **1989**, *90*, 2154.
(15) Pople, J. A.; Head-Gordon, M.; Raghavachari, K. *J. Chem. Phys.* **1987**, *87*, 5968.
(16) Frisch, M. J.; Trucks, G. W.; Schlegel, H. B.; Scuseria, G. E.; Robb, M. A.; Cheeseman, J. R.; Montgomery, J. A., Jr.; Vreven, T.; Kudin, K. N.; Burant, J. C.; Millam, J. M.; Iyengar, S. S.; Tomasi, J.; Barone, V.; Mennucci, B.; Cossi, M.; Scalmani, G.; Rega, N.; Petersson, G. A.; Nakatsuji, H.; Hada, M.; Ehara, M.; Toyota, K.; Fukuda, R.; Hasegawa, J.; Ishida, M.; Nakajima, T.; Honda, Y.; Kitao, O.; Nakai, H.; Klene, M.; Li, X.; Knox, J. E.; Hratchian, H. P.; Cross, J. B.; Adamo, C.; Jaramillo, J.; Gomperts, R.; Stratmann, R. E.; Yazyev, O.; Austin, A. J.; Cammi, R.; Pomelli, C.; Ochterski, J. W.; Ayala, P. Y.; Morokuma, K.; Voth, G. A.; Salvador, P.; Dannenberg, J. J.; Zakraewski, V. G.; Dapprich, S.; Daniels, A. D.; Strain, M. C.; Farkas, O.; Malick, D. K.; Rabuck, A. D.; Raghavachari, K.; Foresman, J. B.; Ortiz, J. V.; Cui, Q.; Baboul, A. G.; Clifford, S.; Cioslowski, J.; Stefanov, B. B.; Liu, G.; Liashenko, A.; Piskorz, P.; Komaromi, I.; Martin, R. L.; Fox, D. J.; Keith, T.; Al-Laham, M. A.; Peng, C. Y.; Nanayakkara, A.; Challacombe, M.; Gill, P. M. W.; Johnson, B.; Chen, W.; Wong, M. W.; Gonzalez, C.; Pople, J. A. *Gaussian 03*, revision A 1; Gaussian, Inc.: Pittsburgh, PA, 2003.
(17) Garrett, G. C.; Truhlar, D. G.; Grev, R. S.; Magnuson, A. W. *J. Phys. Chem.* **1980**, *84*, 1730.
(18) Truhlar, D. G.; Isaacson, A. D.; Garret, B. C. In *Theory of Chemical Reaction Dynamics*, Baer, M., Ed.; CRC Press: Boca Raton, FL, 1985; Vol. 4, p 65.
(19) Lu, D. H.; Truong, T. N.; Melissas, V. S.; Lynch, G. C.; Liu, Y. P.; Garrett, B. C.; Steckler, R.; Issacson, A. D.; Rai, S. N.; Hancock, G. C.; Lauderdale, J. G.; Joseph, T.; Truhlar, D. G. *Comput. Phys. Commun.* **1992**, *71*, 235.
(20) Liu, Y.-P.; Lynch, G. C.; Truong, T. N.; Lu, D.-H.; Truhlar, D. G.; Garrett, B. C. *J. Am. Chem. Soc.* **1993**, *115*, 2408.
(21) Chuang, Y. Y.; Truhlar, D. G. *J. Phys. Chem.* **1997**, *101*, 3808.
(22) Corchado, J. C.; Chuang, Y.-Y.; Fast, P. L.; Hu, W.P.; Liu, Y.-P.; Lynch, G. C.; Nguyen, K. A.; Jackels, C. F.; Ramos, A. F.; Ellingson, B. A.; Lynch, B. J.; Melissas, V. S.; Villà, J.; Rossi, I.; Coitino, E. L.; Pu, J.; Albu, T. V. *Polyrate 9.4*; University of Minnesota, Minneapolis, 2006.
(23) LeBlance, O. H., Jr.; Laurie, V. W.; Gwinn, W. D. *J. Chem. Phys.* **1960**, *33*, 598.
(24) Lide, D. R. *CRC Handbook of Chemistry and Physics*, 80th ed.; CRC Press: New York, 1999.
(25) Nagai, K.; Yamada, C.; Endo, Y.; Hirota, E. *J. Mol. Spectrosc.* **1981**, *90*, 249.
(26) Chen, S.-J.; Chen, C. *J. Mol. Struct. (Theochem)* **2004**, *711*, 57−65.
(27) Chase, M. W., Jr. NIST-JANAF themochemical tables, 4th ed. *J. Phys. Chem. Ref. Data* **1998**, Monograph 9, 1−1951.
(28) Huisman, P. A. G.; Klebe, K. J.; Mijlhoff, F. C.; Renes, G. H. *J. Mol. Struct.* **1979**, *57*, 71.
(29) Shimanouchi, T. *Tables of Molecular Vibrational Frequencies Consolidated Volume I*; National Bureau of Standards: Washington, DC, 1972; pp 1−160.
(30) Jacox, M. E. *J. Mol. Spectrosc.* **1980**, *80*, 257.